

## Improving the performance of industrial TOPCon solar cells through the insertion of intrinsic a-Si layer



S. Ma<sup>a,b</sup>, D.X. Du<sup>a</sup>, D. Ding<sup>a</sup>, C. Gao<sup>a</sup>, Z.P. Li<sup>a</sup>, X.Y. Wu<sup>c</sup>, S. Zou<sup>d</sup>, X. Su<sup>d</sup>, X.Y. Kong<sup>b</sup>, B. Liao<sup>e,\*</sup>, W.Z. Shen<sup>a,\*\*</sup>

<sup>a</sup> Institute of Solar Energy, And Key Laboratory of Artificial Structures and Quantum Control (Ministry of Education), School of Physics and Astronomy, Shanghai Jiao Tong University, Shanghai, 200240, People's Republic of China

<sup>b</sup> School of Materials Science and Engineering, Shanghai Jiao Tong University, Shanghai, 200240, People's Republic of China

<sup>c</sup> School of Photovoltaic and Renewable Energy Engineering, University of New South Wales, Sydney, 2052, Australia

<sup>d</sup> School of Physical Science and Technology, And Jiangsu Key Laboratory of Thin Films, Soochow University, 1 Shizi Street, Suzhou, 215006, People's Republic of China

<sup>e</sup> School of Information Science and Technology, Nantong University, Jiangsu, 226019, People's Republic of China

### ARTICLE INFO

#### Keywords:

Passivating contact  
Polycrystalline silicon  
TOPCon  
Intrinsic amorphous silicon

### ABSTRACT

Passivating contact solar cells have gradually become the mainstream cell technology due to their excellent performance, and further improving the conversion efficiency has become a focus of subsequent research. Typically, achieving excellent field-effect passivation and low contact resistivity in doped polycrystalline silicon (poly-Si) requires heavy phosphorus doping. However, this approach can lead to a predicament wherein excessive phosphorus diffuses into the silicon (Si) substrate during annealing, consequently causing recombination losses. In response to this challenge, a structure incorporating an intrinsic amorphous silicon (a-Si (i)) layer within the passivation layers has been introduced. The primary objective of this structure is to retard the diffusion of phosphorus into the Si substrate. This study entails comprehensive characterizations to delve into the underlying mechanisms of films with the integrated a-Si (i) layer, including surface microscopy, active dopants profile, crystallographic structure, elemental distribution, and electrical properties. Finally, we have fabricated the industrial-sized TOPCon solar cells with an average efficiency of 23.83 %, which is 0.25 % higher than that of Baseline counterparts (23.58 %) on the production line. The above results have demonstrated the introduction of a-Si (i) film can be a buffer layer, retarding the diffusion of phosphorus into the Si substrate and obtaining a better passivation effect, enabling us to further tailor the doping profile for high-efficiency solar cells. Our work highlights a promising strategy to improve the performance of TOPCon solar cells, showcasing the substantial potential for implementation in industrial manufacturing.

### 1. Introduction

Due to the characteristics of renewability and sustainability, solar energy has gradually become a suitable alternative to traditional energy sources [1]. Benefiting from cost advantage, crystalline silicon (c-Si) solar cell technology has dominated the photovoltaic (PV) industry in the past 20 years [2]. Many cell structures have been steadily developed to date, yielding two mainstream technologies for the past few years, i.e., tunnel oxide passivated contact (TOPCon) [3] and heterojunction technology (HJT) [4]. The fabrication of TOPCon can be upgraded from the existing passivated emitter and rear contact (PERC) production lines,

resulting in a record efficiency of 25.8 % on n-type c-Si [5], 26.0 % on p-type c-Si [6], and 26.1 % for an IBC [7] solar cell. Therefore, TOPCon has been considered the next-generation cell technology after PERC [8], which is expected to dominate the PV market in 5 years [9]. The featuring rear passivation layer of TOPCon composed of a heavily doped polycrystalline silicon (poly-Si) layer on ultra-thin silicon oxide ( $\text{SiO}_x$ ,  $\text{Tox}$ ) interlayer has shown superior surface passivation and carrier selectivity by suppressing the recombination at the metal-silicon interface [10] and thus achieving significant efficiency gain [11].

As we know, the excellent surface passivation effect of TOPCon solar cells is attributed to ultrathin  $\text{SiO}_x$  and heavily doped poly-Si layers,

\* Corresponding author.

\*\* Corresponding author.

E-mail addresses: [liaobaochen@ntu.edu.cn](mailto:liaobaochen@ntu.edu.cn) (B. Liao), [wzshen@sjtu.edu.cn](mailto:wzshen@sjtu.edu.cn) (W.Z. Shen).

corresponding to excellent surface chemical passivation and additional field-effect passivation [12], respectively. The key to obtaining the high performance of TOPCon is the preparation of the high-quality tunnel  $\text{SiO}_x$  and heavily doped poly-Si. In terms of Tox, there have been many reports on the methods of preparation, including thermal oxidation [13–16], wet-chemical oxidation [16–18], ozone oxidation [16,17], plasma-assisted oxidation [2,19,20], and plasma-assisted atomic layer deposition (PEALD) [21], resulting in the saturation current density ( $J_0$ ) of  $<3 \text{ fA/cm}^2$  [22,23]. However, most of the above methods cannot be used in industrial production except for thermal oxidation and plasma-assisted oxidation, corresponding to the low-pressure chemical vapor deposition (LPCVD) and plasma-enhanced chemical vapor deposition (PECVD) methods, respectively. Compared to the LPCVD method, the PECVD approach has advantages in high thin film deposition rate, less wrap-round deposition, and equipment-related consumables [22]. The tube PECVD technology integrated with in-situ tunnel  $\text{SiO}_x$  and in-situ doped polysilicon has demonstrated great potential for the mass-production TOPCon in industry [24].

However, amorphous Si (a-Si) film deposited by PECVD is susceptible to poor passivated contacts while the blistering phenomenon occurs during the subsequent annealing process, leading to a significant degradation in device performance [25]. In general, the a-Si film is a technologically important semiconductor for solar cells [26,27], which offers a low defect density and tunable conduction type [28,29]. These optoelectronic advantages strongly rely on configurations of hydrogen and silicon in the three-dimensional space, and thus precise control of its microscopic structure is a critical factor in achieving good devices [30]. While PECVD deposited a-Si often contains a large amount of hydrogen (20 atomic (at.) % and more) from the silicon precursor gas, such as  $\text{SiH}_4$  and  $\text{H}_2$  [31]. Unfortunately, the deposited a-Si film on oxidized Si is strongly prone to blistering, both during deposition and thermal annealing, due to some of the hydrogen from the film accumulating at the film/ $\text{SiO}_x$  interface and growing into pressurized pockets causing the blistering. Blistering deteriorates the properties of the poly-Si/ $\text{SiO}_x$  interface due to the blistered areas being severely hampered, leading to the prevention of charge-carrier collection. In the worst case, blisters may rupture from the surface of poly-Si, resulting in direct contact with the metal electrodes, and thus leading to high recombination loss [32,33]. In summary, the blistering tendency and severity of the a-Si film depend on its H content, thickness, deposition temperature, thermal processing, surface roughness, and cleanliness [32–36]. In addition, interfacial stress accumulation induced during the crystallization of a-Si film has also been related to the occurrence of blistering [37].

Moreover, while adopting the PECVD approach to fabricate TOPCon solar cells, passivating contacts are produced via high-temperature annealing in the range of 850–1000 °C with a dwell time of several tens of minutes to transform the doped a-Si phase into a doped poly-Si phase [38], which guarantees a high field passivation effect. During the annealing process (particularly during the dwell time), dopants in the heavily doped poly-Si layer can diffuse into the c-Si substrate, forming a buried dopant region (called in-diffusion dopant) near the c-Si interface. Although the existence of in-diffusion dopants is beneficial for metal contact to a certain extent and thus reduces contact resistance, however, excessive dopants could severely weaken the interfacial passivation quality. To control dopant diffusion into the Si substrate and attain an optimal equilibrium, it's essential to precisely manage and optimize the dopant concentration within the poly-Si film following the annealing process. Several works [39,40] have investigated the effect of additive intrinsic a-Si layer between  $\text{SiO}_x$  and doped a-Si (p) on the performance of p-TOPCon, indicating that the insertion of intrinsic a-Si layer could effectively regulate the doping distribution in the c-Si/ $\text{SiO}_x$ /doped poly-Si structure, thereby improving the passivation performance of cells. However, it remains to be verified whether this method can achieve similar results for industrialized n-TOPCon.

In this paper, we have introduced a structure with an additional a-Si (i) film to the rear passivation layers of TOPCon solar cells, aiming to

control the phosphorus (P) diffusion into the Si substrate, resulting in a tunable phosphorus doping profile to further improve passivated contact cell performance. Detailed characterizations are carried out to investigate the underlying mechanisms of the films with the introduction of a-Si (i), including surface microscopy, active dopants profile, crystallographic structure, elemental distribution and electrical properties. The morphology of the poly-Si film has been investigated by scanning electron microscope (SEM) and optical microscope (OM) with different thicknesses of introduced a-Si (i) film, revealing the blistering phenomenon occurs when the thickness is 30 nm and above. The active dopant profile results by electrochemical capacitance-voltage profiling (ECV) show that the in-diffusion dopant can be tailored by the introduced a-Si (i) layer. Passivation and contact performance of TOPCon solar cells have been investigated under different thicknesses of a-Si (i) film, and then confirmed the optimal electrical properties at the thickness of 20 nm. Lastly, we have fabricated the industrial-sized TOPCon solar cells with an average efficiency of 23.83 %, which is 0.25 % higher than that of Baseline counterparts (23.58 %) on the production line. These above results have demonstrated the introduction of a-Si (i) can be a good buffer layer, retarding the diffusion of phosphorus towards the Si substrate while enabling us to fine-tune the doping profile and obtain a better passivation effect. Our work has great potential for the mass-production TOPCon solar cells in industry.

## 2. Experimental methods

To evaluate the performance of TOPCon solar cells with the introduced a-Si (i) layer, we fabricated the rear passivation layers on the industrial Czochralski (Cz) n-type silicon wafers with a size of  $182 \times 182 \text{ mm}^2$  (M10), a thickness of  $150 \pm 20 \mu\text{m}$ , and a resistivity of  $0.3\text{--}2.1 \Omega \text{ cm}$ . Characterizations were used to analyze and understand the performance of TOPCon solar cells with different thicknesses of a-Si (i) film.

### 2.1. Fabrication of rear passivation layer

**Fig. 1** describes the fabrication processes of the rear passivated contact structure of TOPCon solar cells. Before the deposition of passivation layers, the n-Si substrate underwent the RCA cleaning to remove the dirt, aiming to ensure final passivation performance. The interfacial ultrathin  $\text{SiO}_x$ , intrinsic a-Si, and in-situ phosphorus-doped a-Si were deposited by a tube-type PECVD system (ZR5000, LeadMicro) at 400 °C with different precursor gases ( $\text{SiO}_x$ :  $\text{N}_2\text{O}$ ; a-Si (i):  $\text{SiH}_4$  and  $\text{H}_2$ ; a-Si (n):  $\text{PH}_3$ ,  $\text{SiH}_4$ , and  $\text{H}_2$ , respectively). A direct radio frequency (RF) plasma source operating at 40 KHz was used. The plasma time of the  $\text{SiO}_x$  process was fixed at 3 min. The total thickness of a-Si was fixed at 140 nm in this study, and the thickness of a-Si (i) and a-Si (n) varied with the respective process time. The annealing process was carried out under nitrogen ( $\text{N}_2$ ) ambient (AS-300E, S.C.) at the temperature of 900 °C for 45 min to transform a-Si to poly-Si and activate the dopants. Lastly, a hydrogenation process was implemented by capping a 100 nm  $\text{SiN}_x$  layer deposited through the PECVD system at 450 °C (PD-405C, S.C.).

### 2.2. Characterization

The surface microscopy of samples was investigated by OM (LEICA DM 4000) and SEM (JSM-7800F). The active dopant depth profile was measured by ECV profiling (WEP, CVP21). Samples with symmetrical structures were prepared to investigate the effective minority carrier lifetime, which was measured by a quasi-steady-state photoconductance method (WCT-120, Sinton Instruments) at an injection density of  $1 \times 10^{15} \text{ cm}^{-3}$ . The single-side  $J_0$  was determined according to the high-injection method proposed by Kane and Swanson [41,42]. The  $i\text{Voc}$  was tested at 1-sun. The contact resistivity ( $\rho_c$ ) was measured by the TLM (Ai-shine). The structural and chemical composition of the c-Si/ $\text{SiO}_x$ /poly-Si interface was investigated by high-resolution transmission electron microscopy (HR-TEM, Talos F200X G2).

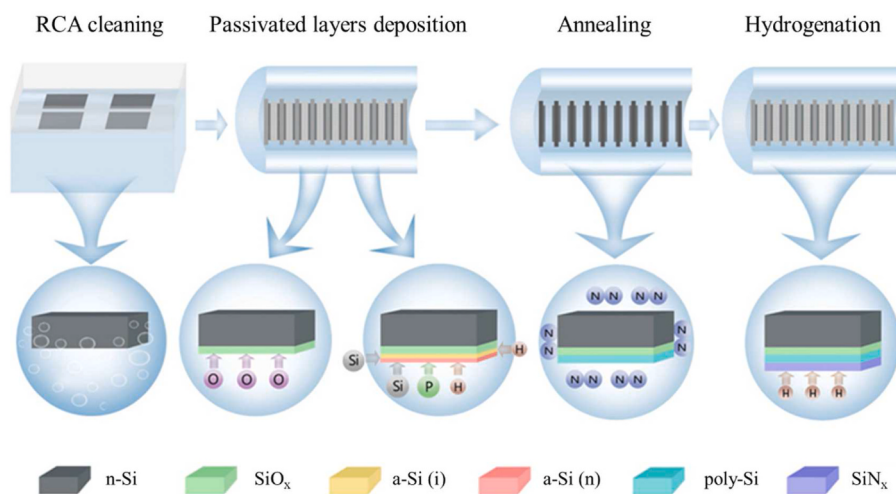


**Fig. 1.** Fabrication processes for poly-Si/SiO<sub>x</sub>/c-Si contacts doped with phosphorus, including the RCA cleaning, PECVD deposition of tunneling oxide, intrinsic a-Si and in-situ phosphorus-doped a-Si, annealing and hydrogenation (deposition of SiN<sub>x</sub>).

Energy-dispersive X-ray spectroscopy (EDS, HP EliteDesk 800 G3 TWR) and secondary ion mass spectroscopy (SIMS, GAIA3) were used to detect related element distributions and intensity for the passivation layers, respectively. The electrical parameters of TOPCon solar cells were measured by Halm 3600 under standard test conditions (AM 1.5G spectrum, 25 °C).

### 3. Results and discussion

In this study, we have introduced the a-Si (i) film as a barrier layer situated between SiO<sub>x</sub>/a-Si (n) layers. The main purpose of this addition is to retard the diffusion of phosphorus into the Si substrate, mitigating the recombination loss that arises from excessive phosphorus diffusion during the annealing process, as previously reported [39]. While the tunneling oxide also contributes to preventing phosphorus diffusion, it's important to note that the passivation contact performance of TOPCon solar cells is highly sensitive to the thickness of the oxide layer. To strike a balance between these competing factors, we have maintained a constant thickness for the tunneling oxide layer throughout this study.

**Fig. 2** illustrates the phosphorus diffusion that occurred during the annealing process, considering varying thicknesses of the a-Si (i) film. In this study, the total thickness of the a-Si film was fixed at 140 nm. The specific thicknesses of the a-Si (i) film were set at 0 nm, 10 nm, 20 nm, 30 nm, and 40 nm, corresponding to the Baseline, G1, G2, G3, and G4 groups respectively. Throughout the annealing process, the a-Si film transformed into poly-Si, and the doped phosphorus became active. After that, the phosphorus atoms initiated diffusion into the Si substrate. As this diffusion progressed deeper, the concentration of phosphorus began to decline after the phosphorus atoms traversed the tunneling oxide layer, and the blocking effect became more potent as the thickness of the a-Si (i) film increased.

When incorporating the a-Si (i) film into the rear passivation layers of TOPCon solar cells, it's crucial to address the blistering issue, particularly when employing the PECVD method. In this study, the samples were prepared on the polished c-Si substrate with different thicknesses of a-Si (i) film by tube PECVD method, and the rear passivation structure corresponded to the groups of Baseline, G1, G2, G3, and G4. To gain insights into the surface characteristics of the

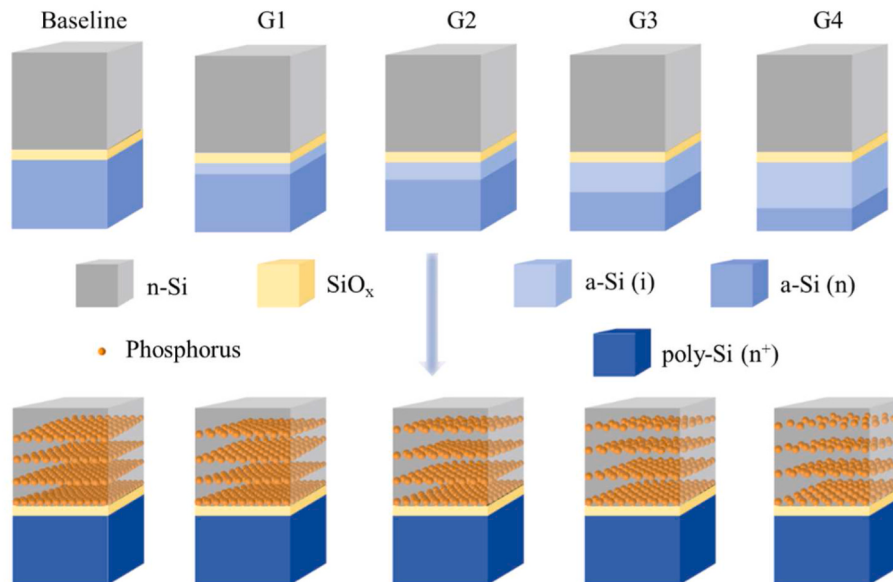


**Fig. 2.** Sketch of phosphorus diffusion into Si substrate during the annealing process with different thicknesses of a-Si (i) film. The thickness of a-Si (i) film was 0 nm, 10 nm, 20 nm, 30 nm, and 40 nm, corresponding to the groups of Baseline, G1, G2, G3, and G4, respectively.

samples before and after the annealing process, OM and SEM were used to observe the surface microscopy of samples with the magnification of 800 and 1500, respectively, as shown in Fig. 3. Observing the images, it was evident that the Baseline, G1, and G2 groups did not exhibit any instances of burst phenomena, suggesting that the presence of phosphorus doping close to the c-Si interface played a role in preventing the a-Si film from bursting during the annealing process. However, as the thickness of the a-Si (i) layer reached a certain value (G3), the surface began to manifest unevenly sized bubbles, which indicated the occurrence of poly-Si film cracking or peeling off from the Si substrate. Comparing the appearance of the film before and after annealing, it was apparent that the annealing process exacerbated the burst phenomenon, leading to larger bubble sizes, which could be attributed to the release and escape of hydrogen (H) during the high-temperature annealing process. When the thickness of the a-Si (i) film was further increased (G4), the size of the burst area was noticeably larger even before annealing. These observations indicated that while heavy phosphorus doping in the a-Si layer could prevent bursting to some extent, the situation changed when the thickness of the a-Si (i) layer exceeded a specific threshold. Beyond this point, the burst phenomenon occurred and worsened as the film's thickness increased.

As reported in the literature, the crystallization of a-Si film leads to the accumulation of interfacial stress and rapid release of hydrogen, which are thought to be the main causes of film blistering [43,44]. Several strategies have been proposed to mitigate this problem, including implementing a slow heat treatment to gradually release hydrogen during the annealing process [34], using Ar instead of H<sub>2</sub> to control the H content or porosity of the film [33,35,45], and combining the elements carbon (C), nitrogen (N), oxygen (O), and phosphorus (P) into the polysilicon film during deposition [2,37,46–48].

To evaluate the influence of the poly-Si with different thicknesses of a-Si (i) film on the TOPCon solar cells, characterizations were conducted on the rear passivation layer. Firstly, we used the ECV method to measure the concentration of active phosphorus within the poly-Si film as shown in Fig. 4(a). It could be seen from the figure that the

concentration of active phosphorus within poly-Si was close to 6E20 cm<sup>-3</sup>. Compared with the group of Baseline, the group of G1 had a similar C-V curve, revealing its analogous blocking effect on phosphorus diffusion. While the thickness of a-Si (i) further increased, the decline curve became steeper, indicating the more obvious blocking effect on phosphorus diffusion. The aforementioned observations substantiated that the doping profile could be accurately regulated through the incorporation of the a-Si (i) layer. To gain a deeper understanding of the performance of the rear passivation layer with varying thicknesses of a-Si (i) film, we conducted investigations into the passivation and contact properties of the TOPCon solar cells. Fig. 4(b) illustrates the symmetrical structure (I) used for testing the  $iV_{OC}$ ,  $J_0$ , and lifetime. Additionally, the semi-manufactured structure (II) designed for measuring contact resistivity ( $\rho_c$ ) using the TLM was presented in the figure. The corresponding results of passivation and contact properties were displayed in Fig. 4(c) and (d), respectively. As seen from Fig. 4(c), when the thicknesses of a-Si (i) increased from 0 nm to 20 nm, the corresponding  $iV_{OC}$  increased from 726.1 mV to 736.6 mV, the lifetime increased from 1028  $\mu$ s to 1729  $\mu$ s, and  $J_0$  decreased from 11.1 fA/cm<sup>2</sup> to 4.3 fA/cm<sup>2</sup>, i.e., the passivation performance of the samples increased in turn. This could be attributed to the few phosphorus atoms diffused to the Si substrate with the increased thickness of a-Si (i), which aligned well with the ECV results. As the thicknesses of a-Si (i) further increased to more than 20 nm, the passivation performance began to slightly decrease, revealing the best result was acquired at the thicknesses of 20 nm. This might be related to the blistering phenomenon of poly-Si film as shown in Fig. 3. In Fig. 4(d), the contact performance of TOPCon solar cells with different thicknesses of a-Si (i) was measured by TLM. The top views of the structures of samples (III) were illustrated in the figure. It could be seen from the figure that when there was no a-Si (i), the measured contact resistivity achieved the minimum value, showing the best contact performance. When the thickness of introduced a-Si (i) increased to 20 nm, the contact resistivity slightly increased, while the thickness exceeded 40 nm, the contact resistivity increased significantly, which could be due to the low concentration of the in-diffusion phosphorus as

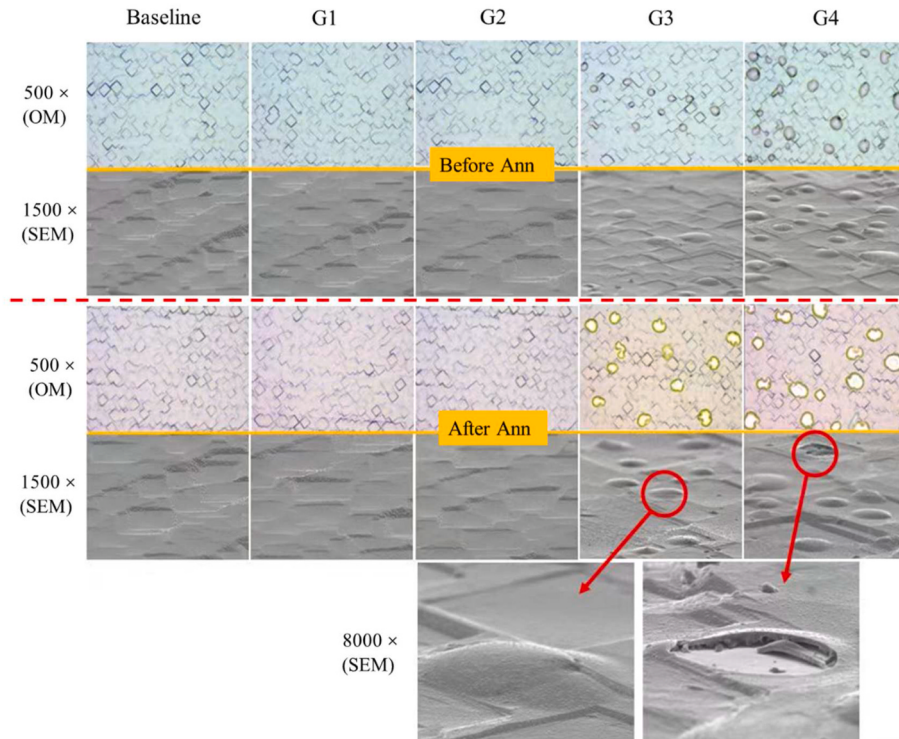


**Fig. 3.** OM photograph and SEM images of the samples before and after annealing. The thickness of a-Si (i) film was 0 nm, 10 nm, 20 nm, 30 nm, and 40 nm, corresponding to the groups of Baseline, G1, G2, G3, and G4, respectively.

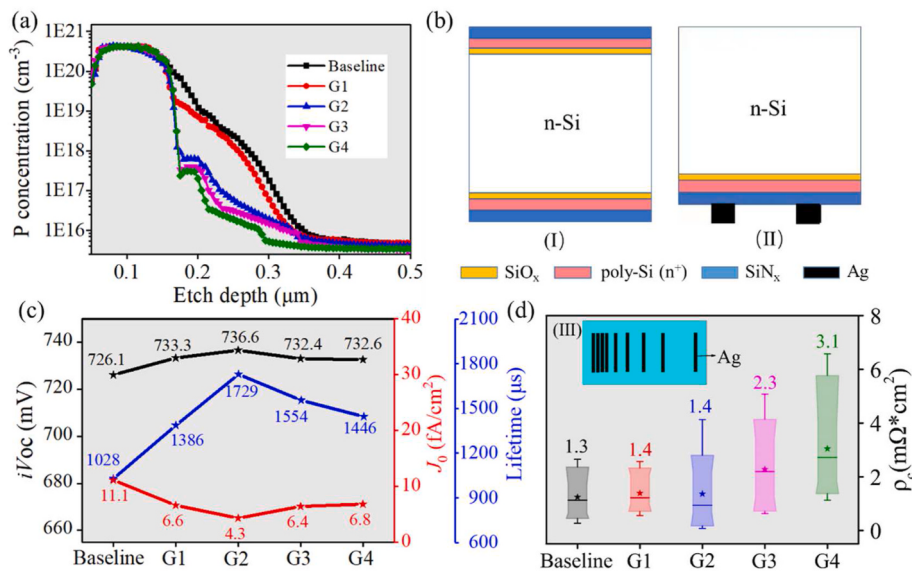


**Fig. 4.** (a) Active phosphorus concentration of samples measured by ECV. (b) The symmetrical structure used to test  $iV_{OC}$ ,  $J_0$ , and lifetime (I), the semi-manufactured structure designed to measure contact resistivity ( $\rho_c$ ) by the TLM (II). (c) The tested  $iV_{OC}$ ,  $J_0$ , and lifetime values were extracted from the symmetrical test samples. (d) Contact resistivity ( $\rho_c$ ) tested by the TLM, together with the top views of the structure of samples (III) illustrated in the figure. The samples were fabricated with different thicknesses of introduced a-Si (i) film, and the thickness was 0 nm, 10 nm, 20 nm, 30 nm, and 40 nm, corresponding to the groups of Baseline, G1, G2, G3, and G4, respectively.

shown in Fig. 4(a). Considering both the passivation and contact performance, it had been established that the TOPCon solar cells achieved the optimal performance with the introduced a-Si (i) of 20 nm. These

research outcomes underscored the value of introducing the a-Si (i) film as a buffer layer, which effectively retarded the diffusion of phosphorus into the Si substrate, leading to enhanced passivation effects. This

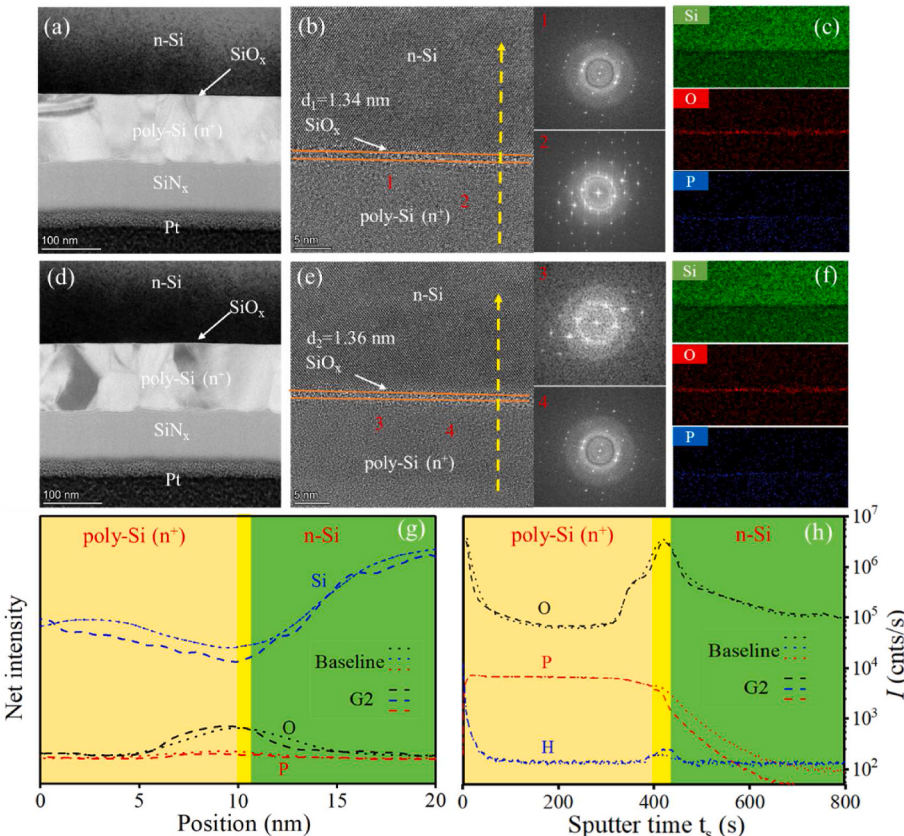


**Fig. 5.** (a and d) TEM images, (b and e) localized TEM images with HR-TEM and Fourier transform diffraction patterns, and (c and f) cross-sectional EDS distributions for the Baseline and G2 samples. (g) Depth-dependent net intensity spectra of Si, O, and P elements. (h) P, H, and O distributions measured by SIMS for the two related samples. Here, the samples were prepared after annealing with the introduced a-Si (i) film at the thickness of 0 nm and 20 nm, corresponding to the groups of Baseline and G2, respectively.

strategic addition allowed for fine-tuning the doping profile, ultimately contributing to the development of high-efficiency solar cells.

To gain a deeper understanding of the impact of the introduced a-Si (i) on the microstructures of poly-Si/SiO<sub>x</sub>/c-Si contacts, HR-TEM analyses were conducted on both the Baseline and optimized G2 groups after the annealing process, and the results were presented in Fig. 5. In the micrographs, the interface tunneling oxide layer displayed a uniform thickness acquired through the PECVD method, and the thickness range of 1.3–1.4 nm for the SiO<sub>x</sub> film was further confirmed by local HR-TEM images. The pronounced crystallization patterns in the poly-Si film were corroborated by distinct diffraction spots evident in the Fourier transform. In contrast to the G2 samples, the Baseline samples exhibited more pronounced polycrystalline structures, alongside amorphous rings with a greater number of discernible diffraction spots. This observation indicated a heightened level of crystallinity following the annealing process [49]. Moreover, the cross-sectional EDS distributions and net intensity for the two related samples were shown in Fig. 5(c and f) and Fig. 5(g), respectively. A phosphorus signal could be observed in the SiO<sub>x</sub> layer and c-Si substrate as shown in Fig. 5(c and f). The cumulative intensity of Si and O atoms across the specific section (yellow dashed line illustrated in Fig. 5(b and e)) indicated the emergence of a tunneling oxide layer. To further investigate the change of O, P, and H atoms after annealing, SIMS was used to detect the intensity of atoms as a function of depth. Fig. 5(h) displayed the SIMS spectra, and the intensity change of O atoms was similar to the results shown in Fig. 5(g). In terms of P atoms, the Baseline group exhibited a notably higher P concentration, particularly after traversing the tunneling oxide layer, which was consistent with the ECV curve shown in Fig. 4(a). These above observations have demonstrated the introduced a-Si (i) layer with an adequate thickness can tailor the doping profile, thereby reducing the recombination loss in the c-Si region, ultimately leading to a better passivated contact cell performance.

In the final evaluation of the introduced a-Si (i) performance at the device level (M10 wafer), TOPCon solar cells were fabricated using passivation layers based on the Baseline, G1, G2, G3, and G4 groups through the TOPCon production line, and the results of electrical parameters were illustrated in Fig. 6. The trend in  $V_{OC}$  variations with different a-Si (i) thicknesses was consistent with the  $iV_{OC}$  measurements. Notably, the G2 group achieved the highest  $V_{OC}$  value of 715 mV, attributed to the blocking effect on phosphorus diffusion. The  $J_{SC}$  value remained unchanged with varying a-Si (i) thickness, implying that the

introduction of a-Si (i) did not lead to additional optical absorption loss. However, the FF value decreased with increasing a-Si (i) thickness, particularly in the G4 group. This reduction was primarily due to the limited diffusion of P atoms into the substrate, resulting in poor metallization contact performance. The most significant observation was the enhancement in conversion efficiency ( $\eta$ ), which improved from 23.58 % to 23.83 % as the a-Si (i) thickness increased from 0 nm to 20 nm. This improvement indicated that the introduction of a-Si (i) could substantially enhance the electrical properties of TOPCon solar cells. On the other hand, when the thickness exceeded 20 nm, both the cell efficiency and  $V_{OC}$  slightly dropped (23.71 % and 23.43 %), potentially due to the blistering phenomenon of poly-Si discussed earlier in Fig. 3. Our research showed that when the thickness of introduced a-Si (i) was 20 nm, the  $\eta$  of TOPCon solar cells improved by 0.25 %, and no blistering was observed simultaneously. These results demonstrated the introduction of a-Si (i) with an adequate thickness was a promising strategy to improve the performance of TOPCon solar cells and has great potential in industrial manufacturing.

#### 4. Conclusions

In summary, this study introduced an additional layer of a-Si (i) layer with a carefully determined thickness, yielding multiple beneficial effects on the performance of TOPCon solar cells. This strategy effectively controlled the doping profile, mitigating the excessive diffusion of phosphorus dopants into the c-Si substrate and consequently reducing recombination losses. Detailed characterizations were carried out to uncover the underlying mechanisms. OM and SEM analyses demonstrated the occurrence of blistering when the a-Si (i) layer thickness reached 30 nm, with increased severity as thickness further increased. Measurements using ECV corroborated the efficient control of in-diffusion dopant by the a-Si (i) layer. The passivation study showed that the optimal performance was obtained at the thickness of 20 nm, with the  $iV_{OC}$  of 736.6 mV and  $J_0$  of 4.3 fA/cm<sup>2</sup>, and the deterioration of passivation beyond 20 nm was attributed to blistering effects. Contact resistivity of 1.4 mΩ cm<sup>2</sup> was extracted from TLM for the introduced a-Si (i) layer with a thickness of 20 nm. In addition, when the thickness of the a-Si (i) layer surpassed 20 nm, there was a significant increment in contact resistance, which could be attributed to the decreased concentration of in-diffused phosphorus within the Si substrate. HR-TEM analyses exhibited the presence of a uniformly thick tunneling oxide at the

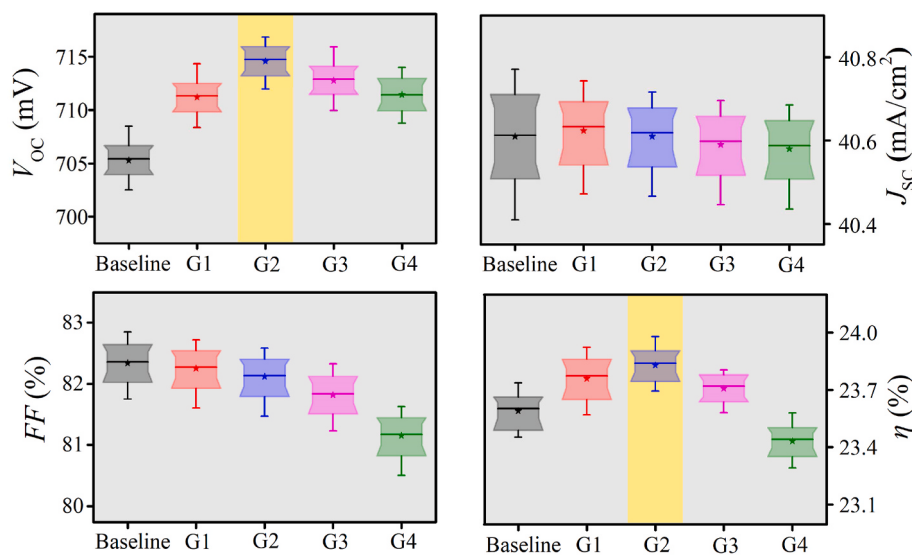


**Fig. 6.** Measured J-V parameters of TOPCon solar cells by adopting different rear passivation layers according to the groups of Baseline, G1, G2, G3, and G4 on the production line using 182 × 182 mm<sup>2</sup> Si wafers. The thickness of a-Si (i) film is 0 nm, 10 nm, 20 nm, 30 nm, and 40 nm, corresponding to the groups of Baseline, G1, G2, G3, and G4, respectively.

interface of c-Si. Additionally, the Fourier transform of the poly-Si film displayed distinct diffraction spots, indicating pronounced crystallization behaviors. Moreover, supplementary elemental studies conducted using EDS and SIMS further confirmed that the in-diffusion phosphorus concentration within the optimal group (G2) was lower compared to the Baseline group. This outcome corroborated the evident blocking effect on phosphorus diffusion, as previously demonstrated through ECV results. Lastly, the industrial M10 TOPCon solar cells were fabricated on the production line, achieving an average efficiency of 23.83 % with the introduced 20 nm a-Si (i) layer, which was 0.25 % higher than that of Baseline counterparts (23.58 %). The above results have demonstrated that the introduction of a-Si (i) to the rear passivation layer was a promising strategy to improve the performance of TOPCon solar cells, and showed tremendous potential in industrial manufacturing.

### CRediT authorship contribution statement

**S. Ma:** Writing – review & editing, Writing – original draft, Methodology, Investigation, Data curation, Conceptualization. **D.X. Du:** Resources, Data curation. **D. Ding:** Resources, Data curation. **C. Gao:** Methodology. **Z.P. Li:** Conceptualization. **X.Y. Wu:** Methodology. **S. Zou:** Conceptualization. **X. Su:** Methodology. **X.Y. Kong:** Visualization, Resources, Conceptualization. **B. Liao:** Writing – review & editing, Supervision, Resources, Methodology, Funding acquisition. **W.Z. Shen:** Writing – review & editing, Supervision, Resources, Funding acquisition, Conceptualization.

### Declaration of competing interest

The authors declare that they have no known competing financial interests or personal relationships that could have appeared to influence the work reported in this paper.

### Data availability

Data will be made available on request.

### Acknowledgments

This work was supported by the Major State Basic Research Development Program of China (Grant No. 2022YFB4200101), the National Natural Science Foundation of China (Nos. 11974242 and 11834011), and the Inner Mongolia Science and Technology Project (Grant No. 2022JBGS0036). B. L. acknowledges the funding support of the Jiangsu Specially-Appointed Professor (Grant No. 06210061007) and the Research Funding for High-level Talents of Nantong University (No. 03083035).

### References

- [1] Y.H. Zeng, H. Tong, C. Quan, Theoretical exploration towards high-efficiency tunnel oxide passivated carrier-selective contacts (TOPCon) solar cells, *Sol. Energy* 155 (2017) 654–660.
- [2] S. Ma, B. Liao, F.Y. Qiao, D.X. Du, D. Ding, C. Gao, Z.P. Li, Q. Wang, X.Y. Wu, S. Zou, X. Su, R.J. Yeo, X. Li, W.M. Li, X.Y. Kong, W.Z. Shen, Bi-layer in-situ phosphorus doped poly-Si films by PECVD for blistering-free high-efficiency industrial TOPCon solar cells, *Sol. Energy Mater. Sol. Cells* 269 (2024) 112771.
- [3] F. Feldmann, B. Steinhäuser, V. Arya, A. Büchler, A.A. Brand, S. Kluska, M. Hermle, S.W. Glunz, Evaluation of TOPCon technology on large area solar cells, in: 33rd European PV Solar Energy Conference and Exhibition, 2017.
- [4] M. Taguchi, A. Yano, S. Tohoda, K. Matsuyama, Y. Nakamura, T. Nishiwaki, K. Fujita, E. Maruyama, 24.7% record efficiency HIT solar cell on thin silicon wafer, *IEEE J. Photovoltaics* 4 (2014) 96–99.
- [5] A. Richter, J. Benick, F. Feldmann, A. Fell, M. Hermle, S.W. Glunz, n-type Si solar cells with passivating electron contact: identifying sources for efficiency limitations by wafer thickness and resistivity variation, *Sol. Energy Mater. Sol. Cells* 173 (2017) 96–105.
- [6] A. Richter, R. Müller, J. Benick, F. Feldmann, B. Steinhäuser, C. Reichel, A. Fell, M. Bivour, M. Hermle, S.W. Glunz, Design rules for high-efficiency both-sides-contacted silicon solar cells with balanced charge carrier transport and recombination losses, *Nat. Energy* 6 (2021) 429–438.
- [7] F. Haase, C. Hollemann, S. Schäfer, A. Merkle, M. Rienäcker, J. Krügener, R. Brendel, R. Peibst, Laser contact openings for local poly-Si-metal contacts enabling 26.1%-efficient POLO-IBC solar cells, *Sol. Energy Mater. Sol. Cells* 186 (2018) 184–193.
- [8] ITRPV, 2021. <https://itrpv.vdma.org/viewer/-/v2article/render/29775594>, 2021.
- [9] W.Z. Shen, Y.X. Zhao, F. Liu, Highlights of mainstream solar cell efficiencies in 2022, *Front. Energy* 17 (2023) 9–15.
- [10] J. Schmidt, R. Peibst, R. Brendel, Surface passivation of crystalline silicon solar cells: present and future, *Sol. Energy Mater. Sol. Cells* 187 (2018) 39–54.
- [11] T.G. Allen, J. Bullock, X. Yang, A. Javey, S.D. Wolf, Passivating contacts for crystalline silicon solar cells, *Nat. Energy* 4 (2019) 914–928.
- [12] A.G. Aberle, S.W. Glunz, A.W. Stephens, M.A. Green, High-efficiency Silicon solar cell: Si/SiO<sub>2</sub> interface parameters and their Impact on Device Performance, *Prog. Photovoltaics Res. Appl.* 2 (1994) 265–273.
- [13] U. Römer, R. Peibst, T. Ohrdes, B. Lim, J. Krügener, T. Wietler, R. Brendel, Ion implantation for poly-Si passivated back-junction back-contacted solar cells, *IEEE J. Photovoltaics* 5 (2015) 507–514.
- [14] D. Yan, A. Cuevas, J. Bullock, Y. Wan, C. Samundsett, Phosphorus-diffused polysilicon contacts for solar cells, *Sol. Energy Mater. Sol. Cells* 142 (2015) 75–82.
- [15] M.K. Stodolny, M. Lenes, Y. Wu, G.J.M. Janssen, I.G. Romijn, J.R.M. Luchies, L. Geerligs, n-type polysilicon passivating contact for industrial bifacial n-type solar cells, *Sol. Energy Mater. Sol. Cells* 158 (2016) 24–28.
- [16] R. Peibst, Y. Larionova, S. Reiter, M. Turcu, R. Brendel, D. Tetzlaff, J. Krügener, T. Wietler, U. Höhne, J.D. Kähler, H. Mehlich, S. Frigge, Implementation of N+ and P+ POLO junctions on front and rear side of double-side contacted industrial silicon solar cells, in: Presented at the 32nd Europ. Photovolt. Sol. Energy Conference, 2016, Munich, Germany.
- [17] A. Moldovan, F. Feldmann, M. Zimmer, J. Rentsch, J. Benick, M. Hermle, Tunnel oxide passivated carrier-selective contacts based on ultra-thin SiO<sub>2</sub> layers, *Sol. Energy Mater. Sol. Cells* 142 (2015) 123–127.
- [18] A. Richter, J. Benick, R. Müller, F. Feldmann, C. Reichel, M. Hermle, S.W. Glunz, Tunnel oxide passivating electron contacts as a full-area rear emitter of high-efficiency p-type silicon solar cells, *Prog. Photovoltaics Res. Appl.* 26 (2018) 579–586.
- [19] M. Jeon, J. Kang, G. Shim, S. Ahn, N. Balaji, C. Park, Y. Lee, J. Yi, Passivation effect of tunnel oxide grown by N<sub>2</sub>O plasma for c-Si solar cell applications, *Vacuum* 141 (2017) 152–156.
- [20] Y.Q. Huang, M.D. Liao, Z.X. Wang, X.Q. Guo, C.S. Jiang, Q. Yang, Z.Z. Yuan, D. D. Huang, J. Yan, X.Y. Zhang, Q. Wang, H. Jin, M. Al-Jassim, C.H. Shou, Y.H. Zeng, B.J. Yan, J.C. Ye, Ultrathin silicon oxide prepared by in-line plasma-assisted N<sub>2</sub>O oxidation (PANO) and the application for n-type polysilicon passivated contact, *Sol. Energy Mater. Sol. Cells* 208 (2020) 110389.
- [21] B. Liao, W.L. Wu, R.J. Yeo, X.Y. Wu, S. Ma, Q. Wang, Y.M. Wan, X.D. Su, W.Z. Shen, X. Li, W.M. Li, G.Q. Xing, B. Hoex, Atomic scale controlled tunnel oxide enabled by a novel industrial tube-based PEALD technology with demonstrated commercial TOPCon cell efficiencies > 24, *Prog. Photovoltaics Res. Appl.* 31 (2022) 220–229.
- [22] D. Yan, A. Cuevas, J.I. Michel, C. Zhang, Y. Wan, X. Zhang, J. Bullock, Polysilicon passivated junctions: the next technology for silicon solar cells? *Joule* 5 (2021) 811–828.
- [23] R. Basnet, D. Yan, D. Kang, M.M. Shehata, P. Phang, T. Truong, J. Bullock, H. P. Shen, D. Macdonald, Current status and challenges for hole-selective poly-silicon based passivating contacts, *Appl. Phys. Rev.* 11 (2024) 011311.
- [24] S. Ma, B. Liao, F.Y. Qiao, D. Ding, C. Gao, Z.P. Li, R. Tong, X.Y. Kong, W.Z. Shen, 24.7% industrial tunnel oxide passivated contact solar cells prepared through tube PECVD integrating with plasma-assisted oxygen oxidation and in-situ doped polysilicon, *Sol. Energy Mater. Sol. Cells* 257 (2023) 112396.
- [25] Q. Yang, M. Liao, Z. Wang, J. Zheng, Y. Lin, X. Guo, Z. Rui, D. Huang, L. Lu, M. Feng, P. Cheng, C. Shou, Y. Zeng, B. Yan, J. Ye, In-situ phosphorus-doped polysilicon prepared using rapid-thermal anneal (RTA) and its application for polysilicon passivated-contact solar cells, *Sol. Energy Mater. Sol. Cells* 210 (2020) 110518.
- [26] A. Shah, P. Torres, R. Tscharner, N. Wyrsch, H. Keppner, Photovoltaic technology: the case for thin-film solar cells, *Science* 285 (1999) 692–698.
- [27] W. Liu, L. Zhang, X. Yang, J. Shi, L. Yan, L. Xu, Z. Wu, R. Chen, J. Peng, J. Kang, K. Wang, F. Meng, S.D. Wolf, Z. Liu, Damp-heat-stable, high-efficiency, industrial-size silicon heterojunction solar cells, *Joule* 4 (2020) 913–927.
- [28] K. Yoshikawa, H. Kawasaki, W. Yoshida, T. Irie, K. Konishi, K. Nakano, T. Uto, D. Adachi, M. Kanematsu, H. Uzu, K. Yamamoto, Silicon heterojunction solar cell with interdigitated back contacts for a photoconversion efficiency over 26, *Nat. Energy* 2 (2017) 1–8.
- [29] A.A. Ashouri, B. Li, A. Magomedov, P. Caprioglio, A. Márquez, A.B.M. Vilches, E. Kasparavicius, J.A. Smith, D. Menzel, M. Grischek, L. Kegelmann, D. Skroblin, C. Gollwitzer, T. Malinauskas, M. Jost, G. Matic, B. Rech, R. Schlatmann, M. Topic, L. Korte, A. Abate, B. Stannowski, D. Neher, M. Stolterfoht, T. Unold, V. Getautis, S. Albrecht, Monolithic perovskite/silicon tandem solar cell with >29% efficiency by enhanced hole extraction, *Science* 370 (2020) 1300–1309.
- [30] V.L. Deringer, N. Bernstein, G. Csányi, C.B. Mahmoud, M. Ceriotti, M. Wilson, D. A. Drabold, S.R. Elliott, Origins of structural and electronic transitions in disordered silicon, *Nature* 589 (2021) 59–64.
- [31] W. Beyer, H. Wagner, The role of hydrogen in a-Si: H-results of evolution and annealing studies, *J. Non-Cryst. Solids* 59–60 (1983) 161–168.
- [32] H.R. Shanks, L. Ley, Formation of pin holes in hydrogenated amorphous silicon at high temperatures and the yield strength of a-Si: H, *J. Appl. Phys.* 52 (1981) 811–813.
- [33] S. Choi, O. Kwon, K.H. Min, M.S. Jeong, K.T. Jeong, M.G. Kang, S. Park, K.K. Hong, H.E. Song, K.H. Kim, Formation and suppression of hydrogen blisters in tunnelling

- oxide passivating contact for crystalline silicon solar cells, *Sci. Rep.* 10 (2020) 9672.
- [34] M. Stohr, J. Aprojanz, R. Brendel, T. Dullweber, Firing-Stable PECVD SiO<sub>x</sub>N<sub>y</sub>/n-poly-Si surface passivation for silicon solar cells, *ACS Appl. Energy Mater.* 4 (2021) 4646–4653.
- [35] A. Morisset, R. Cabal, B. Grange, C. Marchat, J. Alvarez, M.E. Gueunier-Farret, S. Dubois, J.P. Kleider, Highly passivating and blister-free hole selective poly-silicon based contact for large area crystalline silicon solar cells, *Sol. Energy Mater. Sol. Cells* 200 (2019) 109912.
- [36] F. Feldmann, Carrier-Selective Contacts for High-Efficiency Si Solar Cells; Albert-Ludwigs-Universität Freiburg, Freiburg im Breisgau, 2015.
- [37] R. Sharma, A. Alleva, A. Hajjiah, H.S. Radhakrishnan, J. Poortmans, Comparison of C-, N-, and O-incorporated non-blistering PECVD Si films for application in SiO<sub>x</sub>-based passivating contacts for Si solar cells, *ACS Appl. Energy Mater.* 5 (2022) 9994–10001.
- [38] F. Feldmann, M. Simon, M. Bivour, C. Reichel, M. Hermle, S.W. Glunz, Efficient carrier-selective p- and n-contacts for Si solar cells, *Sol. Energy Mater. Sol. Cells* 131 (2014) 100–104.
- [39] J.-I. Polzin, F. Feldmann, B. Steinhauser, M. Bivour, M. Hermle, Annealing and firing stability of in situ boron-doped poly-Si passivating contacts, *AIP Conf. Proc.* 2826 (2023) 020007.
- [40] M.K. Stodolny, J. Anker, C.J.J. Tool, M. Koppes, I.G. Romijn, Novel schemes of Pt poly-Si hydrogenation implemented in industrial 6" bifacial front-and-rear passivating contacts solar cells, in: 35th European Photovoltaic Solar Energy Conference and Exhibition, 2018, pp. 414–417.
- [41] R.A. Sinton, A. Cuevas, Contactless determination of current-voltage characteristics and minority-carrier lifetimes in semiconductors from quasi-steady-state photoconductance data, *Appl. Phys. Lett.* 69 (1996) 2510–2512.
- [42] D.E. Kane, R.M. Swanson, Measurement of the emitter saturation current by a contactless photoconductivity decay method, in: 18th IEEE PVSC, 1985, pp. 578–583.
- [43] B. Nemeth, D.L. Young, M.R. Page, V. Lasalvia, S. Johnston, R. Reedy, P. Stradins, Polycrystalline silicon passivated tunneling contacts for high-efficiency silicon solar cells, *J. Mater. Res.* 31 (2016) 671–681.
- [44] W. Duan, Y. Qiu, L. Zhang, J. Yu, J. Bian, Z. Liu, Influence of precursor a-Si dehydrogenation on the aluminum-induced crystallization process, *Mater. Chem. Phys.* 146 (2014) 141–145.
- [45] D. Yan, S.P. Phang, Y. Wan, C. Samundsett, D. Macdonald, A. Cuevas, High-efficiency N-type silicon solar cells with passivating contacts based on PECVD silicon films doped by phosphorus diffusion, *Sol. Energy Mater. Sol. Cells* 193 (2019) 80–84.
- [46] Y.R. Lin, Z.H. Yang, Z.K. Liu, J.M. Zheng, M.M. Feng, Y.Y. Zhi, L.N. Lu, M.D. Liao, W. Liu, D. Ma, Q.L. Han, H. Cheng, Q.S. Zeng, Z.Z. Yuan, B.J. Yan, Y.H. Zeng, J. H. Ye, Dual-functional carbon-doped polysilicon films for passivating contact solar cells: regulating physical contacts while promoting photoelectrical properties, *Energy Environ. Sci.* 14 (2021) 6406–6418.
- [47] Q. Yang, Z.K. Liu, Y.R. Lin, W. Liu, M.D. Liao, M.M. Feng, Y.Y. Zhi, J.M. Zheng, L. N. Lu, D. Ma, Q.L. Han, H. Cheng, Z.H. Yang, K. Ding, W. Duan, H. Chen, Y. Wang, B.J. Yan, Y.H. Zeng, J.H. Ye, Passivating contact with phosphorus-doped polycrystalline silicon-nitride with an excellent implied open-circuit voltage of 745 MV and its application in 23.88% efficiency TOPCon solar cells, *Sol. RRL* 5 (2021) 2100644.
- [48] J.K. Zhou, X.L. Su, Q. Huang, Y.H. Zeng, D. Ma, W. Liu, B.J. Yan, J.C. Ye, J. Yang, X.Y. Zhang, H. Jin, Y. Zhao, G.F. Hou, Approaching 23% efficient n-type crystalline silicon solar cells with a silicon oxide-based highly transparent passivating contact, *Nano Energy* 98 (2022) 107319.
- [49] Y. Wada, S. Nishimatsu, Grain growth mechanism of heavily phosphorus-implanted polycrystalline silicon, *J. Electrochem. Soc.* 125 (1978) 1499–1504.